Rapamycin Inhibits Growth of Premalignant and Malignant Mammary Lesions in a Mouse Model of Ductal Carcinoma *In situ*

Ruria Namba,[1] Lawrence J.T. Young,[2] Craig K. Abbey,[3] Lisa Kim,[2] Patrizia Damonte,[2] Alexander D. Borowsky,[1,2] Jinyi Qi,[3] Clifford G. Tepper,[4] Carol L. MacLeod,[5] Robert D. Cardiff,[1,2] and Jeffrey P. Gregg[1]

Abstract

Purpose: Rapamycin has been shown to have antitumor effects in various tumor models. To study the effect of rapamycin at different stages of breast cancer development, we used two unique mouse models of breast cancer with activated phosphatidylinositol 3-kinase (PI3K) pathway. Met-1 tumors are highly invasive and metastatic, and mammary intraepithelial neoplasia-outgrowths (MIN-O), a model for human ductal carcinoma *in situ*, are transplantable premalignant mammary lesions that develop invasive carcinoma with predictable latencies. Both of these models were derived from mammary lesions in Tg(*MMTV-PyV-mT*) mice.

Experimental Design: Met-1 tumors were used to study the effect of rapamycin treatment on invasive disease. Transplanted MIN-O model was used to study the effect of rapamycin on premalignant mammary lesions. Animals were *in vivo* micro – positron emission tomography imaged to follow the lesion growth and transformation to tumor during the treatment. Cell proliferation, angiogenesis, and apoptosis was assayed by immunohistochemistry.

Results: Rapamycin inhibited *in vitro* tumor cell proliferation and *in vivo* Met-1 tumor growth. The growth inhibition was correlated with dephosphorylation of mammalian target of rapamycin (mTOR) targets. Rapamycin treatment significantly reduced the growth of the premalignant MIN-O lesion, as well as tumor incidence and tumor burden. Growth inhibition was associated with reduced cell proliferation and angiogenesis and increased apoptosis.

Conclusions: In PyV-mT mouse mammary models, rapamycin inhibits the growth of premalignant lesions and invasive tumors. Although the inhibitory effect of rapamycin was striking, rapamycin treatment did not completely obliterate the lesions.

Originally used as antifungal agent and a suppressor of the immune system, rapamycin has recently been studied as an anticancer agent. Rapamycin inhibits mammalian target of rapamycin (mTOR), a serine/threonine kinase, by binding to its immunophilin, FK-binding protein (FKBP12; reviewed refs. 1, 2). In breast cancer, rapamycin offers significant promise as many of the pathways dysregulated in this disease are mTOR related (3). Of particular recent interest are the phosphatidylinositol 3-kinase (PI3K) and Akt pathways. Breast cancer cell lines overexpressing ErbB2, which is amplified in 30% of human breast cancer (4), are sensitive to rapamycin (5). In addition, cell lines with high activation level of Akt, a downstream target of ErbB2, are similarly sensitive to rapamycin (5, 6). Rapamycin has also been shown to reverse Akt-derived resistance to tamoxifen (7, 8). In general, there is a correlation of Akt pathway activation and rapamycin sensitivity in breast cancer cells (5).

The inhibitory effect of rapamycin and its derivatives on *in vivo* tumor progression has been recently suggested by several studies (9 – 11). In K-ras-mutated mice that have activated PI3K/Akt signaling, mTOR inhibition reversed tumor progression of lung adenocarcinoma (11). In the prostate, Akt-induced mouse prostatic intraepithelial neoplasia was reversed by mTOR inhibitor treatment (10). In breast cancer, rapamycin therapy was found to reduce or inhibit mammary tumor development in a transgenic ErbB2 mouse model (9).

In this study, two transplantable mouse tissue models, with activated PI3K/Akt pathway, were used to study the effectiveness of rapamycin on preinvasive (premalignant) and invasive mammary lesions. The transplantable lesions originated from

Authors' Affiliations: [1]Department of Pathology and Laboratory Medicine, School of Medicine; [2]Center for Comparative Medicine; Departments of [3]Biomedical Engineering and [4]Biochemistry and Molecular Medicine, University of California, Davis; and [5]National Cancer Institute, Bethesda, Maryland

Received 10/5/05; revised 1/27/06; accepted 2/14/06.

Grant support: National Cancer Institute grants R01-CA89140-01 (R.D. Cardiff and J.P. Gregg), CA81376 (C.L. MacLeod), and R21-CA102733 (C.K. Abbey); California Breast Cancer Research Program grants 11IB-0123 (J.P. Gregg) and 9FB-0212 (R. Namba); and Small Animal Imaging Resource Program grant R24 CA 110804.

The costs of publication of this article were defrayed in part by the payment of page charges. This article must therefore be hereby marked *advertisement* in accordance with 18 U.S.C. Section 1734 solely to indicate this fact.

Note: Processing and immunohistochemistry of fixed tissue was done in the mutant mouse pathology laboratory (Center for Comparative Medicine, University of California, Davis). The small animal magnetic resonance imager was on-loan from Systems Associates, Inc. (Libertyville, IL).

Requests for reprints: Jeffrey P. Gregg, Department of Pathology and Laboratory Medicine, School of Medicine, University of California, Davis, Room 2460, MIND Wetlab Building, 2805 50th Street, Sacramento, CA 95817. Phone: 916-703-0362; Fax: 916-703-0367; E-mail: jpgregg@ucdavis.edu.

doi:10.1158/1078-0432.CCR-05-2170

Tg(*MMTV-PyV-mT*) female mammary fat pads (12, 13) and have high levels of Akt activation. Tg(*MMTV-PyV-mT*) model mimic the biology of human breast cancer (14, 15). The Tg(*MMTV-PyV-mT*) mammary fat pad develops multifocal tumors at 100% penetrance with multistage development of mammary invasive carcinoma (atypical, hyperplastic, invasive, and metastatic). Although PyV-mT is not an endogenous oncogene, it acts as a molecular surrogate for ErbB2, an oncogene associated with breast cancer, to activate ErbB2-related signaling pathways, including PI3K/Akt pathway (16). Tg(*MMTV-PyV-mT*) tumors have high PI3K activity (17). The molecular biology and histopathology of PyV-mT mouse mammary lesions also strongly resemble human breast cancer (13–15, 18–20).

To isolate and study the premalignant stage, we used transplantable mammary intraepithelial neoplasia-outgrowth (MIN-O) tissue lines derived from hyperplastic mammary lesions in young Tg(*MMTV-PyV-mT*) females (13). The resulting lesions develop in an immunocompetent setting and mimic the biological behavior, molecular biology, and histopathology of human ductal carcinoma *in situ* (13, 19) and fulfill the NIH Annapolis Pathology Panel criteria for premalignant intraepithelial lesions (21). The tissue transplant lines have been maintained *in vivo* by serial transplantation to mammary gland–cleared wild-type host fat pads. When allowed to develop, these lesions will continue to grow within the boundary of the host mammary fat pad and tumor foci will develop within the outgrowth at latencies that can be predicted with varying degrees of precision by phenotype (13). Recently, this model was used to evaluate and compare the chemopreventive effects of a novel selective estrogen receptor modulator, ospemifene, with tamoxifien (22).

To study invasive disease, the Met-1 tumor line, derived from a mammary tumor of Tg(*MMTV-PyV-mT*) female (12), was used. It has been maintained as an *in vivo* transplantable tumor line, as well as an *in vitro* tumor cell culture line (12). Met-1 tumors are highly invasive and metastatic (12, 23).

These two mouse models of breast cancer were used to investigate the effects of rapamycin at different stages of development. We evaluated the effect of rapamycin on cell proliferation in *in vitro* Met-1 tumor cell lines. For *in vivo* studies, the transplanted tissues from *in vivo* rapamycin treatments were analyzed with immunohistochemistry to assess cell proliferation, angiogenesis, and apoptosis. *In vivo* imaging was used to monitor the longitudinal development of lesions with and without rapamycin treatment.

Rapamycin significantly decreased *in vitro* cell proliferation and *in vivo* tumor growth in the invasive cancer model. In the transplanted MIN-O model, growth was significantly reduced and this was associated with inhibition of cell proliferation and angiogenesis and increased apoptosis. These data suggest that rapamycin or its analogues are potential effective therapeutics for both preneoplastic (e.g., human ductal carcinoma *in situ*) and invasive breast cancer.

Materials and Methods

Animals

Tg(*MMTV-PyV-mT*) mice (24) were bred and maintained at the University of California, Davis. *FVB* females were purchased from Charles River Laboratories (Wilmington, MA). Met-1 tumor (12) and MIN-O (13) serial transplant lines were maintained at University of California, Davis.

For *in vivo* Met-1 tumor studies, 1 mm^3 pieces of the donor Met-1 tumor were transplanted to no. 4 mammary fat pads of 3-week-old *FVB* females bilaterally. For MIN-O studies, 1 mm^3 pieces of the 8w-B MIN-O tissues (13) were transplanted to gland-cleared no. 4 mammary fat pads of 3-week-old *FVB* females bilaterally.

Animals were maintained in University of California, Davis, vivarium according to NIH guidelines, and all procedures were conducted under institutionally approved animal protocols.

Cell proliferation assay

Cell culture conditions for Met-1 tumor cells was described previously (12). Cells were plated in 96-well plates at a density of 1,000 per well in 100 μL complete DMEM medium with 10% fetal bovine serum overnight. A 50 mmol/L rapamycin (Calbiochem, San Diego, CA) stock solution was prepared in DMSO and stored at −20°C. The stock solution was diluted with PBS to make 20× working solutions. The culture medium was replaced with rapamycin-containing medium (0.01, 0.1, and 1 μmol/L rapamycin) or vehicle control medium (0.005% DMSO in fresh medium). Forty-eight hours after the addition of rapamycin-containing medium, relative cell growth was determined using the CellTiter 96 cell proliferation assay kit (Promega, Madison, WI).

Immunoblot analysis

MIN-Os and tumor tissues were snap frozen in liquid nitrogen and stored at −80°C. Frozen tissues were homogenized in lysis buffer [10 mmol/L Tris buffer (pH 7.6)], with protease inhibitor (Sigma, St. Louis, MO), caspase inhibitor, and phosphatase inhibitor (Calbiochem) with a Dounce homogenizer. The extracts were incubated at 4°C for 10 minutes and centrifuged at 10 krpm for 30 minutes at 4°C. Met-1 tumor cells were seeded in a six-well plate (0.3×10^6 per well) overnight. Cells were treated with 10 nmol/L rapamycin for 6 hours and harvested according to previously published protocol (12). Protein concentration was determined using BCA assay kit (Promega). Thirty micrograms of protein were resolved by SDS-PAGE and transferred onto polyvinylidene difluoride membranes (Millipore, Billerica, MA) and probed with the following antibodies: Akt, phospho-Akt (Ser^{473}), phospho-4E-BP1 (Ser^{67}), phospho-p70S6K (Thr^{389}), p70S6K (all 1:1,000) and cyclin D1 (1:2,000; Cell Signaling Technology, Beverly, MA), and β-actin (1:2,500, Sigma). The following secondary antibodies were used: horseradish peroxidase–conjugated anti-mouse and anti-rabbit (Amersham Bioscience, Piscataway, NJ). The signal on the membranes was detected using Supersignal (Promega) on a gel documentation system (Alpha Innotech, San Leandro, CA).

Rapamycin treatment

Rapamycin (LC Laboratories, Woburn, MA) was dissolved in ethanol at a concentration of 50 mg/mL and stored at −20°C. The rapamycin solution was freshly prepared by diluting the rapamycin stock in a 1:1 10% PEG-400, 8% ethanol:10% Tween 80 solution to make a 100 μL dose per animal (9). Animals were treated by i.p. injection every other day for the duration of the treatment. Control animals received i.p. injection of vehicle (100 μL of 5% PEG-400, 4% ethanol, and 5% Tween 80) every other day. Rapamycin injection (0.75 mg/kg dose) i.p. had been shown to have antitumor effect in MMTV-neu transgenic animals (9).

In vivo Met-1 tumor studies

Rapamycin treatment was started when the transplanted Met-1 tumors became palpable at 14 days posttransplantation. Animals were treated at 0.19, 0.75, 3.0, or 12.0 mg/kg doses for 21 days (four animals and eight tumors per group). During the treatment, tumor size was measured in two dimensions using a digital caliper until the vehicle-treated control tumors reached 1.5 cm in diameter. Tumor size was calculated using the formula (length × $width^2$) / 2. At the end of the

study, small pieces of the tumors were flash frozen and the remaining tumor tissue was fixed in 10% formalin.

To detect and quantitate small tumors at the early phase of rapamycin treatment, animals transplanted with Met-1 tumor pieces were imaged with magnetic resonance imaging (MRI) at 2 days before the start of treatment and 7th and 14th day of the treatment ($n = 8$ for each group). Rapamycin treatment (3.0 mg/kg dose) was started on 14 days posttransplantation.

MIN-O studies

Thirty-five-day rapamycin treatment. MIN-O-transplanted animals were treated with 0.19, 0.75, and 3.0 mg/kg doses of rapamycin as well as vehicle control ($n = 3$ for control, 0.19 and 0.75 mg/kg doses, $n = 4$ for 3.0 mg/kg dose). The treatment was started at 7 days after transplantation and continued for 35 days. At the end of the treatment, MIN-O size and tumor size, if any, were recorded, and the fat pads were fixed for whole-mount analysis according to previously published methods (25).

Positron emission tomography study. At 30 days posttransplantation, rapamycin treatment started at the 3.0 mg/kg dose (5 animals and 10 MIN-O transplants). Control animals (5 animals and 10 transplants) were treated with vehicle only. All animals were micro–positron emission tomography (PET) imaged immediately before the beginning of the rapamycin treatment and at 7th and 14th day of the treatment.

Seven-day rapamycin treatment. For immunohistochemistry analysis, MIN-O-transplanted animals were treated with 3.0 mg/kg dose (7 animals and 14 transplants) or with vehicle control (4 animals and 8 transplants) starting at 21 days posttransplantation. After 7 days of treatment, the animals were sacrificed and the MIN-O tissues were snap-frozen and the remaining fat pads were fixed for histology.

Three-hour rapamycin treatment. For immunohistochemistry analysis for apoptosis, MIN-O-transplanted animals were treated with 3.0 mg/kg dose (four animals and eight transplants) or vehicle control (two animals and four transplants) at 21 days posttransplantation. Three hours after the treatment, the animals were sacrificed and the MIN-O tissues were fixed for histology.

In vivo imaging techniques

MRI and PET were used to assess lesion properties over multiple time points in longitudinal studies.

A low-field benchtop MRI system (MagnuVu MV500 MRI system, SAI, Libertyville, IL) was used to assess the volume of *in vivo* Met-1 tumors. Animals were anesthetized (0.6 mg/kg body weight; Nembutal) and imaged with a T1, 22-slice protocol using a DICOM compression. Tumor volume was calculated using 3D-Image analysis software (3D-Doctor, Able Software, Lexington, MA). The system gives reasonably high-resolution scans ($0.8 \times 0.8 \times 0.5$ mm) in a convenient benchtop configuration and allows quantitation of small tumors that are difficult to measure with a digital caliper.

In the MIN-O lesions, it was important to establish the premalignant stage at treatment onset while the lesions were not yet palpable. We chose to evaluate the effects of rapamycin *in vivo* using the small-animal PET imaging technique previously shown to discriminate premalignant from malignant tissue in the MIN-O model (26). Animals were scanned on a dedicated small-animal PET scanner (micro-PET Focus system, CTI Concorde, Knoxville, TN) using the glucose analogue 2-[^{18}F]fluoro-deoxy-D-glucose. The scanner resolution is ~1.3 mm (center of FOV) with sensitivity >4%. The scanning protocol called for animals to be anesthetized, injected with 200 to 300 μCi 2-[^{18}F]fluoro-deoxy-D-glucose, and held 30 minutes for biodistribution of the tracer before commencing with a 30-minute scan. List-mode scanner data was converted to a sinogram and then reconstructed using an iterative maximum *a posteriori* reconstruction algorithm (27, 28). This reconstruction algorithm has been shown to remove or substantially reduce streaking artifacts lateral of the bladder that would normally obscure the no. 4 mammary fat pads (29). After reconstruction, the volumetric images were normalized to uptake in the brain of the animal. This normalization is used because extravasated tracer is often found at the injection site making the injected dose unreliable (29).

Immunohistochemistry

The tissues were fixed in 10% formalin and processed for H&E and immunohistochemistry by the University of California, Davis, Pathology Laboratory. Four-micrometer-thick paraffin sections were stained with Mayer's H&E or immunostained with the following antibodies as described previously: anti-Ki-67, anti-CD31 (20), and anti-cleaved caspase-3 (1:250; Promega).

Quantitation of cell proliferation, microvessels, and apoptosis

Cell proliferation was visualized with anti-Ki-67. Magnification images (×40) of the proliferative zone ($n = 20$ for control and $n = 22$ for rapamycin) and the differentiating zones ($n = 15$ for control and $n = 25$ for rapamycin) from four control fat pads and five rapamycin-treated fat pads were analyzed. Using the Image-Pro Plus software (Media Cybernetics, Silver Spring, MD), Ki-67-positive nuclei were quantitated as percentages of total nuclei.

Microvessels in the fat pads were visualized with anti-CD31. Thirty ×40 magnification images from three fat pads were analyzed for both control and rapamycin-treated animals. Using the Image-Pro Plus software, CD31-positive area was measured as a percentage of total area.

Apoptosis was visualized with anti-cleaved caspase-3. Ten 40× magnification images from four rapamycin-treated fat pads and five images from two control fat pads were analyzed. Number of caspase-3-positive cells and total number of nuclei were counted in each image. Apoptotic cell counts were normalized by the total number of cells per image.

Statistical analysis

All statistical analysis was carried out using an unpaired *t*-test analysis in GraphPad Prism 4 software (GraphPad Software, San Diego, CA).

Results

PyV-mT mammary tumors have activated mTOR pathway. Because PyV-mT mammary tumors have activated the PI3K/Akt pathway (12, 17), we expected these tumors to have activated mTOR and be responsive to mTOR inhibition. Rapamycin sensitivity of PyV-mT mammary tumors was initially assessed *in vitro* by treating Met-1 tumor cells with this agent. Rapamycin treatment inhibited Met-1 tumor cell proliferation by 30% (Fig. 1A). As expected, rapamycin-treated Met-1 cells had significantly lower levels of phosphorylated p70S6K and a decreased level of overall p70S6K protein (Fig. 1B). Rapamycin treatment also reduced phosphorylation of 4E-BP1, another downstream target of mTOR, at residue Ser^{65} known to be rapamycin sensitive. Phosphorylation of 4E-BP1 at Thr^{37} and Thr^{46}, phosphorylation of which are insensitive to rapamycin, was not affected. As rapamycin is known to induce G_1 arrest by blocking the translation of mRNAs of cell cycle proteins (2, 30), the level of cyclin D1, a G_1-S cyclin, was reduced in the rapamycin-treated Met-1 cells.

***Rapamycin inhibits growth of Met-1 tumors* in vivo.** Because rapamycin effectively inhibited cell proliferation *in vitro*, the effect of rapamycin on *in vivo* mammary tumor growth was studied using animals with Met-1 tumors transplanted to their mammary fat pads. Rapamycin treatment was initiated when the tumors became palpable. To determine the optimal dosage for treatment, different rapamycin concentrations were used to treat the animals. In the first experiment, animals transplanted with Met-1 tumors were treated with three doses of rapamycin

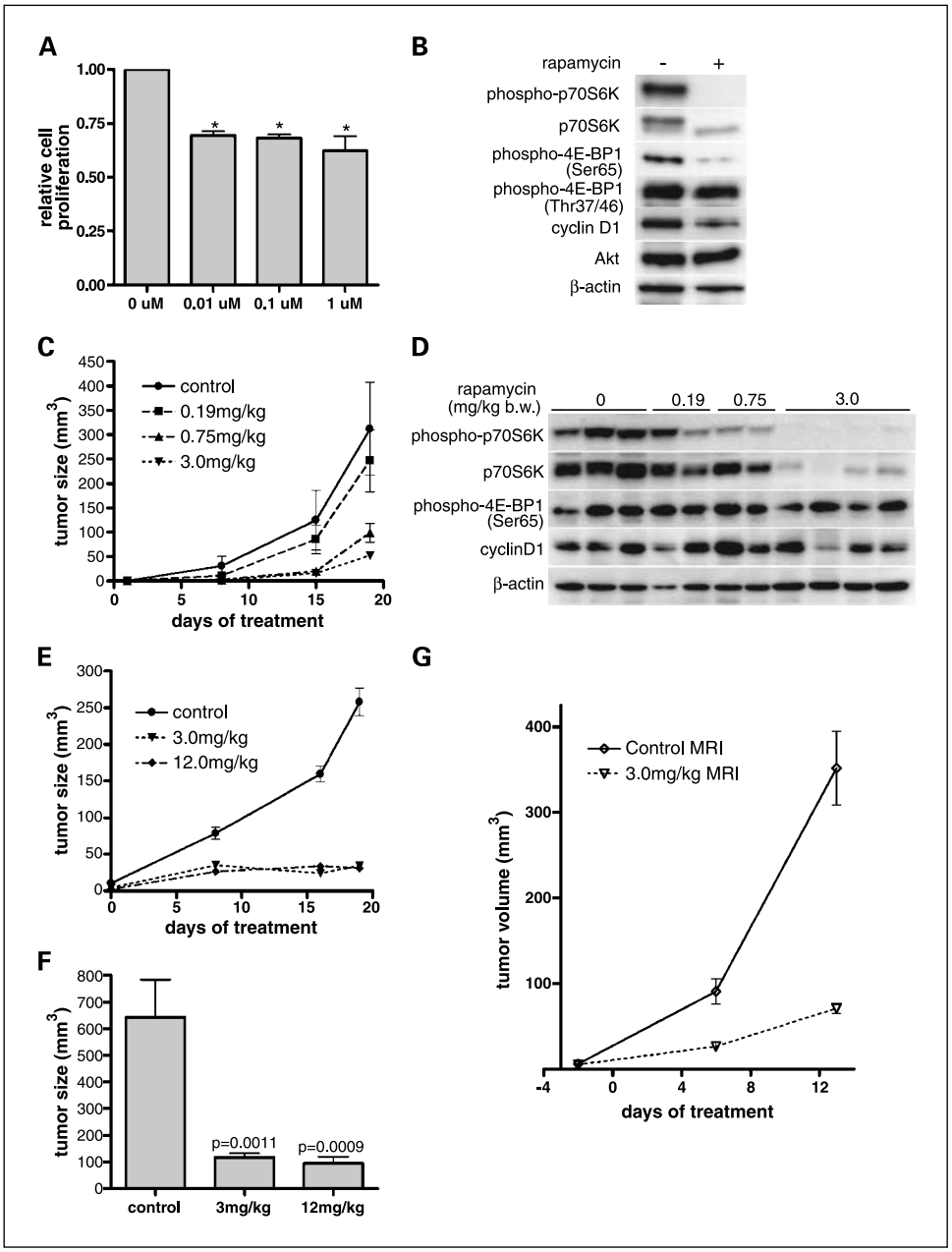

Fig. 1. Met-1 tumor *in vitro* and *in vivo* rapamycin treatment. *A* and *B*, Met-1 tumor cells were treated with rapamycin *in vitro*. *A*, Met-1 tumor cell proliferation is sensitive to rapamycin in a dose-dependent manner. Cell proliferation was significantly reduced 48 hours after rapamycin treatment (*, $P < 0.001$) *B*, Western blot of protein extracts from Met-1 tumor cells after 6 hours of rapamycin treatment. Rapamycin treatment inhibited the activation of p70S6K and 4E-BP1. *C* to *G*, Met-1 tumor – transplanted animals were treated with various doses of rapamycin. *C* and *D*, Met-1 tumor – transplanted animals were treated with 0.19 mg/kg (■, $n = 8$), 0.75 mg/kg (▲, $n = 8$), 3.0 mg/kg (▼, $n = 8$), or vehicle only (●, $n = 6$). *C*, rapamycin treatment resulted in dose-dependent antitumor effect with 3.0 mg/kg dose showing the most effective tumor growth inhibition. Tumor size was measured using a digital caliper. *D*, tumor protein extracts from each group were resolved on a SDS-PAGE gel and phosphorylation status of mTOR targets, p70S6K, and 4E-BP1, as well as total protein levels of p70S6K and cyclin D1, were detected. *E* and *F*, Met-1 tumor – transplanted animals were treated with 3.0 mg/kg (▼, $n = 8$), 12.0 mg/kg (◆, $n = 8$), or vehicle only (●, $n = 8$). *E*, tumor size was measured using a digital caliper starting at the beginning of the treatment. *F*, after 21 days of treatment, all animals were terminated and the excised tumor size was measured with a digital caliper. Average tumor sizes of both treatment groups were significantly smaller than that of the vehicle control group. *G*, Met-1 tumor – transplanted animals were MRI imaged starting 2 days before the beginning of the rapamycin treatment (rapamycin; ▽, $n = 8$, vehicle control; ◇, $n = 8$). All transplants, which were not palpable at the beginning of the study, could be detected and quantitated using the MRI system.

(0.19, 0.75, and 3.0 mg/kg body weight; Fig. 1C and D). After 14 days of rapamycin treatment, tumors in rapamycin-treated animals were smaller than the tumors in untreated animals. The effectiveness of rapamycin was dose-dependent, with the 0.19 mg/kg dose showing the least growth-inhibitory effect. In the second experiment, Met-1 tumor-bearing animals were treated with two different rapamycin doses (3.0 or 12.0 mg/kg body weight; Fig. 1E and F). Again, tumors were smaller than the tumors in the control group at 7 days of treatment. Tumor mass remained small or even continued to decrease in size for the duration of the treatment. The final tumor sizes of these two groups of rapamycin-treated animals were significantly smaller than those of the control animals and the tumor sizes between these two treatment groups were not significantly different (Fig. 1F).

To more accurately measure the effect of rapamycin on early time points of the treatment, before the tumors were palpable, Met-1 tumor – transplanted animals were imaged with small animal MRI (Fig. 1G). With MRI, we were able to detect and quantitate all tumors, including those that were nonpalpable, at 2 days before the start of the treatment. After 7 days of treatment, the rapamycin-treated tumors were significantly smaller ($P = 0.003$) than the vehicle-treated tumors.

The phosphorylation status of mTOR targets in the Met-1 tumors from the rapamycin-treated animals was assessed by Western blot (Fig. 1D). Rapamycin treatment inhibited the phosphorylation of p70S6K in a dose-dependent manner. With 3.0 mg/kg dose, phosphorylation of p70S6K was almost completely inhibited. Rapamycin also reduced the total level of p70S6K protein. The phosphorylation of 4E-BP1 as well as

the cyclin D1 level was only slightly reduced in tumors from the 3.0 mg/kg dosage group.

Rapamycin inhibits growth of premalignant mammary lesions. Because rapamycin was effective in inhibiting mammary tumor growth, we tested its chemopreventive effect on premalignant mouse mammary lesions. Animals transplanted with MIN-O were treated with 0.19, 0.75, and 3.0 mg/kg body weight doses. After 35 days of rapamycin treatment, MIN-O sizes were smaller in all doses of rapamycin-treated animals compared with the MIN-Os in the vehicle-treated control animals (Fig. 2A and B). In the control animals, transplanted MIN-Os had grown to fill over 60% of the no. 4 mammary fat pad (Fig. 2A) and each MIN-O transplant had developed at least one tumor focus (Fig. 2B). With the 0.75 and 3.0 mg/kg dosages, the MIN-O size was significantly smaller than with the control. Compared with the control MIN-Os, which were clearly visible under the dissecting microscope, rapamycin-treated MIN-Os were difficult to identify because of their small size (<20% fat pad filled) and pale appearance. Among all rapamycin-treated MIN-Os, only one was found to have a small tumor focus (1 mm in diameter; data not shown). These results suggest that rapamycin treatment reduces the growth of premalignant mouse mammary lesions and inhibits the malignant transformation of these lesions.

As the MIN-O lesions and small tumor foci are not palpable, size and premalignant/malignant status is difficult to quantitate without the surgical exposure of the host mammary fat pads. Previously, micro-PET imaging has been useful to study the growth and tumor progression of the MIN-Os (26). The MIN-O-transplanted animals were imaged using micro-PET weekly for 3 weeks, starting just before the beginning of the treatment (Fig. 3). Before the treatment, the MIN-Os were detectable by micro-PET within the area of the no. 4 fat pad. The uptake of the MIN-Os was within the range of their previously observed uptake level (26). After 7 days of rapamycin treatment, the lesion volume and the maximum uptake of the lesions decreased from the previous scan, whereas in the vehicle control animals, MIN-O size and uptake continued to increase. The functionally active volume of lesions in the controls increased by ~80% in this time, whereas that in the treatment group decreased by a factor of at least 400% to a size less than the volumetric resolution of the scanner. The two cohorts were not significantly different before the treatment onset ($P > 0.1$, two-sample t-test, $df = 16$), but achieved statistical significance ($P < 0.001$) in both measures after the 7 days of treatment. After 14 days of treatment, the lesion volume and 2-[^{18}F]fluoro-deoxy-D-glucose uptake remained at low levels, whereas those in the controls continued to increase. The treated lesions remained small in volume and the maximum 2-[^{18}F]fluoro-deoxy-D-glucose uptake level remained below the level before the rapamycin treatment, indicating that the lesions did not transform into tumors during this period. The control lesions grew larger and, based on their size and the high maximum uptake level, had transformed into tumors. Therefore, in the rapamycin-treated MIN-Os, the major effect on the biology occurred during the 1st week of treatment (signified by a significant loss of volume and 2-[^{18}F]fluoro-deoxy-D-glucose uptake compared with the week prior and the controls), whereas in the 2nd week, the volume and uptake remained unchanged ($P > 0.1$, paired t-test, $df = 10$).

To investigate the mechanisms mediating the early rapamycin-induced changes observed after 7 days of treatment in the micro-PET studies, a second cohort of MIN-O-transplanted animals were similarly treated (i.e.,, 3 mg/kg) to study the molecular and pathologic changes. The rapamycin treatment started at 3 weeks posttransplantation. Typically at 3 weeks posttransplantation, the transplanted MIN-Os have grown to fill ~30% to 40% of the fat pad filled without the development of tumor foci. After 7 days of treatment, the MIN-Os from rapamycin-treated animals were

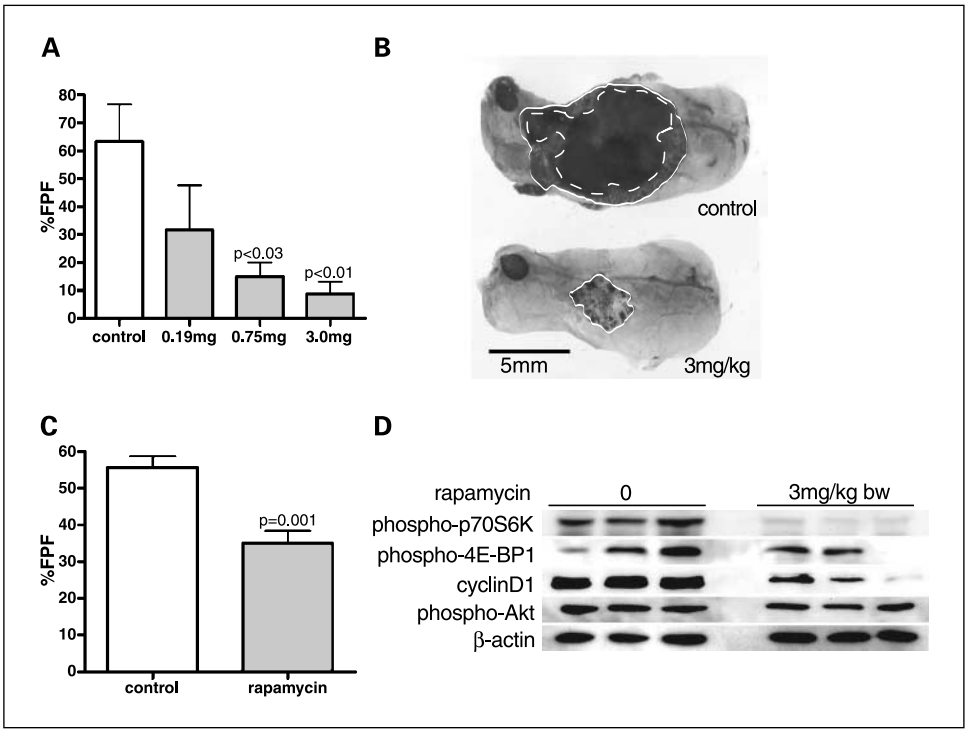

Fig. 2. MINO *in vivo* rapamycin treatment. *A* and *B,* MIN-O-transplanted animals were treated with three different doses of rapamycin, starting 1 week posttransplantation. *A,* the MIN-O sizes were significantly smaller compared with the controls after 35 days of treatment at 0.75 and 3.0 mg/kg doses ($n = 3$ for each group except for the 3.0 mg/kg dose, which were $n = 4$). *B,* representation of MIN-Os from vehicle-treated control animals and from the rapamycin-treated animals. The MIN-O from vehicle-treated control animal filled over 60% of the fat pad area (*solid line*) and had tumor foci (*dashed line*). The MIN-O from rapamycin-treated animal was smaller (*solid line*) and had no tumor foci. *C* and *D,* MIN-O-transplanted animals were treated with 3 mg/kg dose of rapamycin for 7 days ($n = 8$ for controls and $n = 16$ for rapamycin), starting 3 weeks posttransplantation. *C,* the rapamycin-treated MIN-Os were significantly smaller ($P = 0.001$) compared with the vehicle-treated controls. *D,* Western blots of rapamycin-treated and vehicle-treated MIN-Os. Three different tissues from each group were resolved on a SDS-PAGE gel. Activation of p70S6K and expression of cyclin D1 is inhibited by rapamycin treatment *in vivo*. The inhibition of 4E-BP1 activation is not as pronounced as that of the p70S6K.

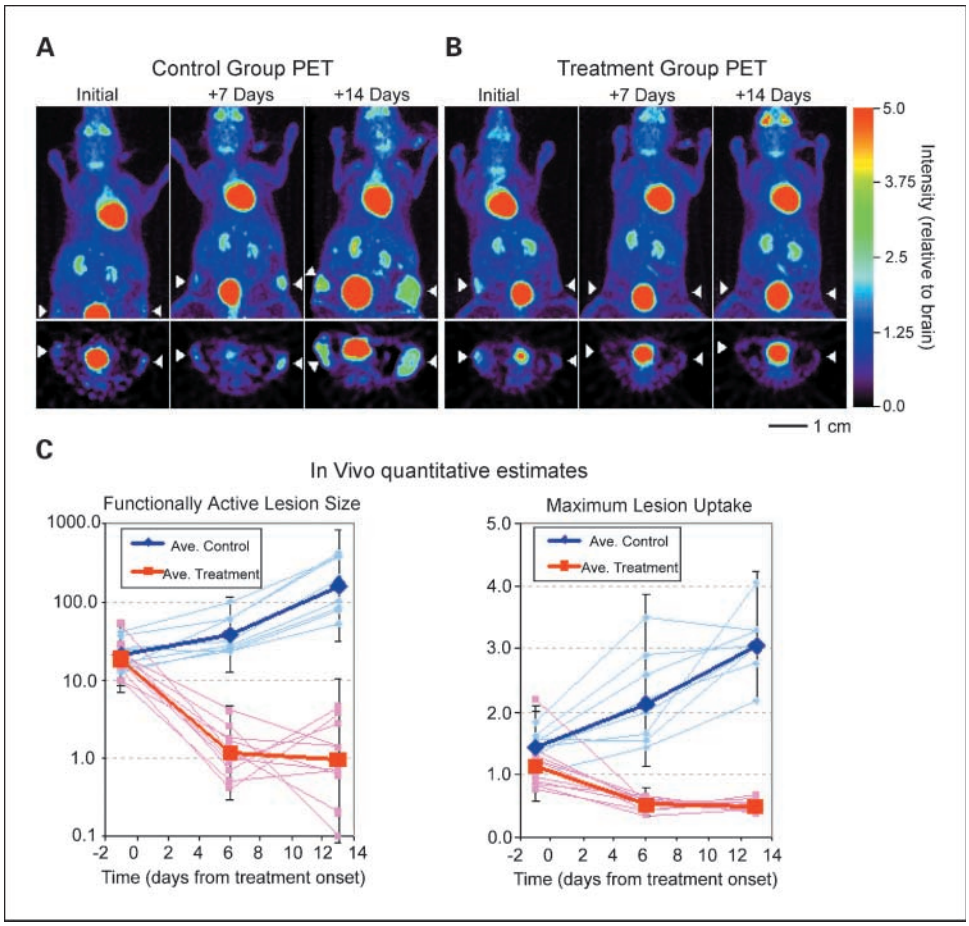

Fig. 3. *In vivo* PET imaging of rapamycin-treated MIN-Os. Longitudinal panels of representatives from control (*A*) and treatment (*B*) groups. Each panel consists of coronal maximum intensity projections and a transverse slice from the lesion area (*arrows*). Quantitative estimates of the volume and maximum uptake of functionally active tissue in the lesions were extracted from the three-dimensional reconstructed images and plotted in (*C*). *Pale red and blue points,* individual lesions from treatment and control cohorts, respectively. *Points,* average values for each cohort; *bars,* 95% confidence interval (*in bold*).

significantly smaller (35% fat pad filled) than the MIN-Os from the vehicle-treated control animals (55% fat pad filled; Fig. 2C). Interestingly, the MIN-Os from rapamycin-treated animals were pale and not as dense in appearance compared with the untreated MIN-Os under the dissecting microscope (data not shown).

Activation status of mTOR signaling effectors in the MIN-Os were studied using protein extracts from these samples (Fig. 2D). In untreated MIN-Os, both downstream effectors of mTOR, p70S6K, and 4E-BP1 were phosphorylated as well as Akt. Rapamycin treatment effectively suppressed the phosphorylation of p70S6K and 4E-BP1, and reduced the expression of cyclin D1, but did not affect Akt phosphorylation.

Histologic changes in the rapamycin-treated MIN-Os. The transplanted MIN-Os proliferate to fill the mammary fat pad and differentiate to form duct-like structures and small dysplastic cysts. In the growing MIN-Os, the proliferative and differentiation zones can be distinguished morphologically and have distinct characteristics (Fig. 4A). The proliferative zone is composed of collections of cells with slightly larger nuclei and greater discohesion than the differentiated zone. These nests of cells are reminiscent of normal terminal end buds, the proliferative distal ends of the normal developing mammary tree. By comparison to the normal terminal end buds, the MIN-O-proliferative zone is denser and the individual end buds are generally larger by 50% to 100%. The proliferative zone, therefore, constitutes the most peripheral area of the MIN-O extending roughly 15 to 20 cell diameters from the leading edge of MIN-O growth into the host mammary fat pad. The differentiation zone, in turn, displays a greater degree of architecture, with cells showing greater polarity, and more abundant cytoplasm. Differentiation patterns vary, but duct and small cyst-like structures predominate. By comparison to the normal developing ductal trees, the cytology is more dysplastic, the epithelial cellularity is more dense, and normal appearing slender ducts lined by uniform epithelium are absent. Finally, the invasive carcinomas that arise from the MIN-Os arise in the differentiation zone, near the center of the outgrowth. This finding implies that the transplanted MIN tissue undergoes a progression from proliferation to differentiation to transformation. In mammary fat pads from rapamycin-treated animals, MIN-Os were not only smaller but also sparse (i.e., small clusters of epithelium were found scattered within the host stroma), compared with the dense MIN-Os in the fat pads from untreated animals (Fig. 4B).

Cell proliferation and angiogenesis was quantitated with immunohistochemistry. Because the proliferative and differentiation zones may have different responses to the rapamycin treatment, the immunohistochemistry staining in these zones was scored separately. Anti-Ki-67 was used as a marker for cell proliferation (Fig. 4C-E). In the proliferative zone, average percentage of Ki-67-positive cells was 86% in untreated MIN-Os and 72% in rapamycin-treated MIN-Os (Fig. 4C, E, and H). In the differentiation zone, there was less cell proliferation than the proliferative zone (51% in untreated versus 41% in rapamycin; Fig. 4D, E, and H). In both areas, rapamycin-treated MIN-Os had

less Ki-67-positive cells. The differences in cell proliferation rates were statistically significant in both zones as well as when both zones were considered together.

Rapamycin has been shown to inhibit angiogenesis in various tumor models (9, 31). We suspected that MIN-Os in rapamycin-treated animals are less vascular due to their pale appearance under the dissecting microscope. To determine the effect on angiogenesis, MIN-O-bearing fat pads were stained with anti-CD31 antibody (Fig. 4F and G). The CD-31-positive area was >30% smaller in rapamycin treated than in the untreated MIN-O tissues in both the proliferative and differentiation zones (Fig. 4I). This suggests that the rapamycin treatment resulted in reduced angiogenesis in the MIN-O tissues.

Apoptosis rate quantitated by anti-cleaved caspase-3 immunohistochemistry did not show significant differences between rapamycin-treated and untreated MIN-O tissues after 7 days of rapamycin treatment (data not shown). We speculated that the rapamycin treatment may result in rapid induction of apoptosis and the apoptotic response is completed by 7 days of treatment. To test this hypothesis, we analyzed the apoptosis incidence in MIN-O tissues 3 hours after the rapamycin treatment (Fig. 4J). In the rapamycin-treated MIN-Os, the number of caspase-3-positive cells was significantly increased ($P = 0.004$) compared with the untreated MIN-O tissues.

Discussion

In this study, we asked whether rapamycin has growth inhibitory effects on invasive and premalignant mammary lesions. We found that rapamycin can effectively inhibit growth of invasive tumors and premalignant lesions in PyV-mT-based mouse models, which have activated PI3K/Akt

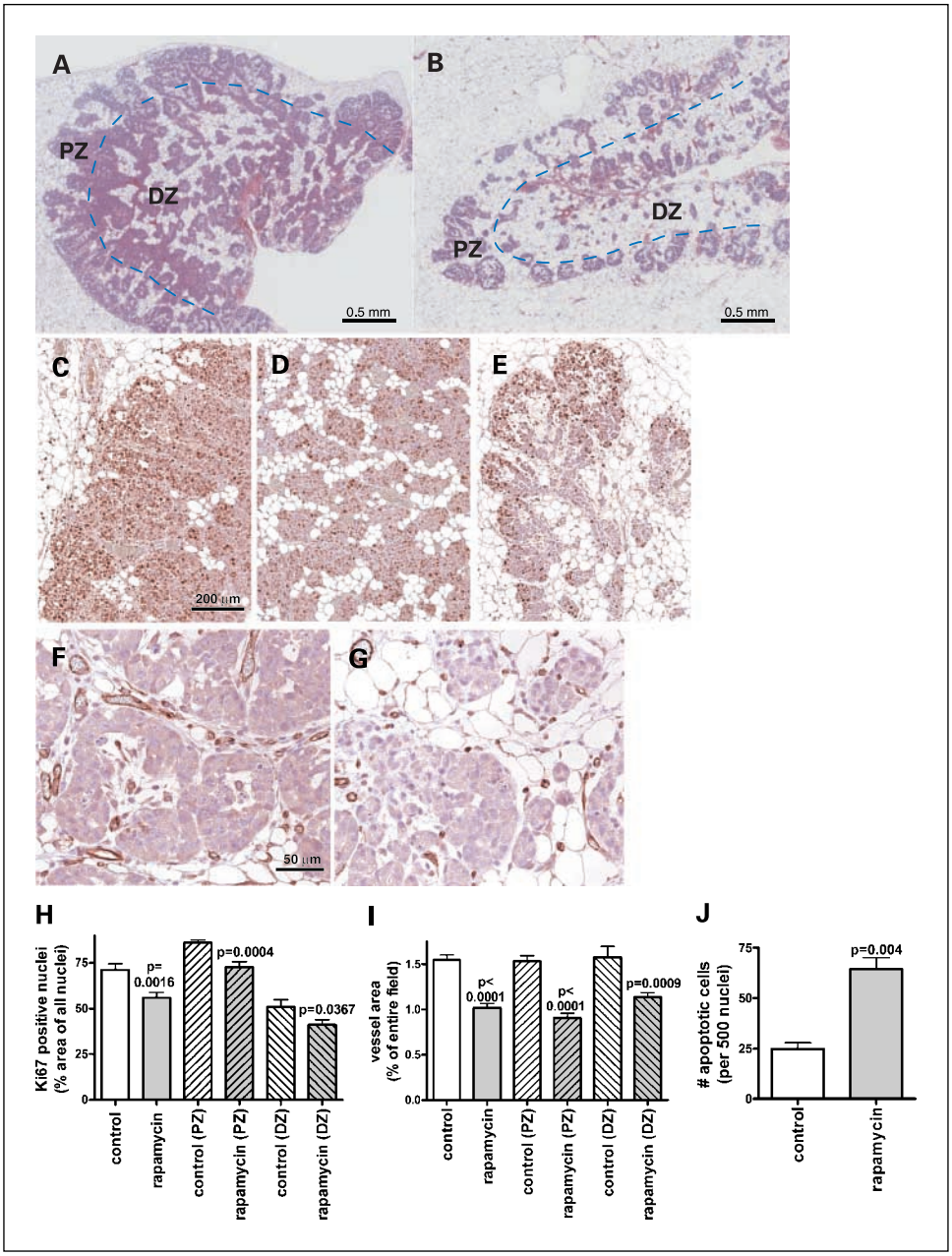

Fig. 4. Histology of untreated and rapamycin-treated MIN-Os. H&E-stained paraffin sections of MIN-Os from vehicle-treated control (*A*) and rapamycin-treated (*B*) animals. *A,* two zones, proliferation zone (*PZ*) and differentiation zone (*DZ*), can be distinguished within the MIN-O tissue (*separated by blue lines*). *B,* MIN-Os from the rapamycin-treated animals are smaller and have less dense epithelium. Magnification, ×4. *C* to *E, H,* cell proliferation was scored by anti-Ki-67. Ki-67-positive cells (*brown*) are highly abundant in the proliferating zone of vehicle-treated MIN-Os (*C*), whereas the differentiation zone (*D*) has fewer Ki-67-positive cells. In the rapamycin-treated MIN-Os (*E*), a higher proportion of Ki-67-positive cells are found at the edge of the MIN-Os than in the center. Overall, rapamycin-treated MIN-O had fewer Ki-67-positive cells than untreated MIN-Os (*D*). Magnification, ×10. *F, G*, and *I,* microvessels were quantitated by anti-CD31 in MIN-Os from vehicle-treated (*F*) and rapamycin-treated (*G*) animals. Rapamycin-treated MIN-Os had less CD31-positive area than the control MIN-Os (*I*). Magnification, ×40. *J,* apoptosis was quantitated by anti-cleaved caspase-3 in MIN-Os, 3 hours posttreatment of the animals. Rapamycin-treated MIN-Os had significantly higher apoptotic cell counts than the vehicle-treated MIN-Os.

pathway (12, 13). The *in vivo* rapamycin treatment resulted in dephosphorylation of mTOR target proteins in a dose-dependent manner.

Rapamycin treatment inhibited the growth of PyV-mT-induced carcinomas (Met-1 tumors). Tumor cell proliferation was inhibited by 30% *in vitro*, whereas the tumor size was 80% smaller at the end of the *in vivo* rapamycin treatment study. The treatment, however, did not completely abolish the malignant lesions even after 3 weeks of continuous treatment. Thus, rapamycin has significant growth inhibitory effect on tumors, but it does not cause total growth inhibition or ablation of these tumors. This suggests that the treatment of invasive carcinoma with rapamycin maybe more effective in a combinational therapy with cytotoxic compounds, such as apoptosis-inducing agents or cell killing agents. Recently, a rapamycin derivative, RAD001, was shown to sensitize tumor cells to cisplatin-induced apoptosis (32). A cytotoxic agent, paclitaxel, has also been shown to have synergistic effects with rapamycin in breast cancer cells (33). Moreover, combinational therapies with inhibitors of other pathways, such as pamidronate (farneysylation pathway inhibitor; ref. 34) and letrozole (aromatase inhibitor; ref. 35), have been shown to be effective in breast cancer cell lines.

Rapamycin treatment had more dramatic effects on the premalignant MIN-Os than on the Met-1 invasive carcinoma model. The treated premalignant transplants were significantly smaller and had significantly lower tumor incidence and tumor burden than the vehicle-treated MIN-O transplants. This suggests that rapamycin may have inhibitory effects on the progression to invasive carcinoma. Recently, in transgenic mouse mammary tumor models with activated ErbB2, rapamycin was shown to have chemopreventive effects when treated before the emergence of palpable tumors (9). In a mouse prostate model with activated Akt, rapamycin treatment resulted in reversal of a PIN phenotype (10). In addition to growth inhibitory effects on premalignant and malignant lesions, these results suggest a promising chemopreventive effect of rapamycin, especially in lesions with activated Akt.

In vivo imaging was used to follow the growth of the nonpalpable MIN-O lesions during the rapamycin treatment. After 7 days of rapamycin treatment, a dramatic decrease in the functionally active lesion volume was detected compared with the size of the MIN-O lesion before the treatment and to the vehicle-treated control. After 14 days of treatment, the MIN-O size remained small but did not continue to decrease in size. This *in vivo* imaging data suggests that the major effects of rapamycin had occurred early during the 1st week of treatment with a later maintenance (antiproliferative or cytostatic) phase. In addition, these data showed that the *in vivo* PET imaging technique can be used for assessing effectiveness of interventions, when traditional assessment methodologies (i.e., palpation) cannot be used.

Histologic changes after 7 days of rapamycin treatment was also studied to better understand the early changes that resulted from the continuous rapamycin treatment. The typical untreated MIN-Os have two distinct zones that reflect the biology of the MIN-Os. Cells at the edge of the MIN-O tissue, at the host stroma interface, represent the growing margin of the outgrowth, similar to the terminal end bud that represents the proliferating tissue. As the mammary tissue grows by peripheral extension, the cells away from the edge differentiate to form various structures, such as dysplastic cysts and solid nests of cells. Because the edges of the MIN-Os are highly proliferative, the majority (over 80%) of cells in this "proliferating zone" stained for Ki-67. In the more central "differentiation zone," noticeably fewer proliferating cells exist than in the proliferative zone, yet ~50% of cells were positive for the Ki-67 proliferation marker.

The rapamycin treatment affected the two zones slightly differently. In general, rapamycin reduced cell proliferation, but had an especially pronounced antiproliferative effect on the highly proliferative cell populations, which are at the stroma-epithelium interface. This zonal effect of rapamycin maybe partly due to changes in stromal environment as a result of the rapamycin treatment.

Rapamycin treatment reduced the microvessel density in the MIN-O-transplanted mammary fat pads indicating that angiogenesis was significantly effected. Interestingly, at 1 week of treatment, immunohistochemistry for active caspase-3 did not show a change in the apoptosis pattern (data not shown), but immediately after the rapamycin treatment, the apoptosis incidence was significantly increased. In the micro-PET imaging, there is clearly reduction in the functionally active lesion volume over 7 days of rapamycin treatment. But after 7 days, the MIN-Os did not continue to decrease in size significantly. Therefore, rapamycin result in a rapid induction of apoptosis in our model and the majority of this process is completed after 7 days.

In the MIN-Os, rapamycin inhibited both the p70S6K and 4E-BP1 phosphorylation, as well as decreased the total cyclin D1 level. The inhibition of cyclin D1 expression seems to be via a posttranscriptional mechanism because the cyclin D1 transcript level in the rapamycin-treated MIN-Os was not significantly changed (data not shown). This is consistent with a previous study showing that the rapamycin suppressed cyclin D1 translation in cells with high Akt activity (36). Compared with the Met-1 tumors, 4E-BP1 phosphorylation in the MIN-Os was more sensitive to the rapamycin treatment. This suggests that Met-1 tumors have developed an alternative mechanism for 4E-BP1 phosphorylation or inhibition of dephosphoryation (e.g., reduced PP2A activity; ref. 37) that may explain why the premalignant lesions seem to be more responsive to the antigrowth effect of rapamycin than the invasive carcinoma.

In summary, we show that in a PyV-mT mouse mammary carcinoma model, rapamycin inhibits the growth of premalignant lesions as well as invasive tumors. The suppressive effect seems to be caused by reduced cell proliferation and angiogenesis, and increased apoptosis. Although the inhibitory effect of rapamycin was striking, in both premalignant and tumor models, we did not see complete obliteration of lesions by the rapamycin treatment. Thus, rapamycin may not be effective as a sole chemotherapy or chemopreventive, but it may affect basic machinery of premalignant or tumor cells enough so that the cells may become significantly susceptible for a second therapy, such as tamoxifen, or standard chemotherapeutics, such as cisplatin or Adriamycin. Application of rapamycin in a combinational therapy should be investigated.

Acknowledgments

We thank Robert Munn for histology image processing and advice on analysis; the Center for Molecular and Genomic Imaging at University of California, Davis, for micro-PET imaging; the members of the Gregg Laboratory and the pathology laboratory for technical assistance, especially Stephenie Liu for rapamycin treatment and for critical reading of the manuscript and Leo Lee and Richelle Enriquez for technical assistance.

References

1. Bjornsti MA, Houghton PJ. The TOR pathway: a target for cancer therapy. Nat Rev Cancer 2004;4:335–48.
2. Hidalgo M, Rowinsky EK. The rapamycin-sensitive signal transduction pathway as a target for cancer therapy. Oncogene 2000;19:6680–6.
3. Carraway H, Hidalgo M. New targets for therapy in breast cancer: mammalian target of rapamycin (mTOR) antagonists. Breast Cancer Res 2004;6:219–24.
4. Slamon DJ, Clark GM, Wong SG, et al. Human breast cancer: correlation of relapse and survival with amplification of the HER-2/neu oncogene. Science 1987;235:177–82.
5. Yu K, Toral-Barza L, Discafani C, et al. mTOR, a novel target in breast cancer: the effect of CCI-779, an mTOR inhibitor, in preclinical models of breast cancer. Endocr Relat Cancer 2001;8:249–58.
6. DeGraffenried LA, Fulcher L, Friedrichs WE, et al. Reduced PTEN expression in breast cancer cells confers susceptibility to inhibitors of the PI3 kinase/Akt pathway. Ann Oncol 2004;15:1510–6.
7. Campbell RA, Bhat-Nakshatri P, Patel NM, et al. Phosphatidylinositol 3-kinase/AKT-mediated activation of estrogen receptor α: a new model for anti-estrogen resistance. J Biol Chem 2001;276:9817–24.
8. Pietras RJ, Arboleda J, Reese DM, et al. HER-2 tyrosine kinase pathway targets estrogen receptor and promotes hormone-independent growth in human breast cancer cells. Oncogene 1995;10:2435–46.
9. Liu M, Howes A, Lesperance J, et al. Antitumor activity of rapamycin in a transgenic mouse model of ErbB2-dependent human breast cancer. Cancer Res 2005;65:5325–36.
10. Majumder PK, Febbo PG, Bikoff R, et al. mTOR inhibition reverses Akt-dependent prostate intraepithelial neoplasia through regulation of apoptotic and HIF-1-dependent pathways. Nat Med 2004;10:594–601.
11. Wislez M, Spencer ML, Izzo JG, et al. Inhibition of mammalian target of rapamycin reverses alveolar epithelial neoplasia induced by oncogenic K-ras. Cancer Res 2005;65:3226–35.
12. Borowsky AD, Namba R, Young LJT, et al. Syngeneic mouse mammary carcinoma cell lines: two closely related cell lines with divergent metastatic behavior. Clin Exp Metastasis 2005;22:47–58.
13. Maglione JE, McGoldrick ET, Young LJ, et al. Polyomavirus middle T-induced mammary intraepithelial neoplasia outgrowths: single origin, divergent evolution, and multiple outcomes. Mol Cancer Ther 2004;3:941–53.
14. Lin EY, Jones JG, Li P, et al. Progression to malignancy in the polyoma middle T oncoprotein mouse breast cancer model provides a reliable model for human diseases. Am J Pathol 2003;163:2113–26.
15. Maglione JE, Moghanaki D, Young LJ, et al. Transgenic polyoma middle-T mice model premalignant mammary disease. Cancer Res 2001;61:8298–305.
16. Dilworth SM. Polyoma virus middle T antigen and its role in identifying cancer-related molecules. Nat Rev Cancer 2002;2:951–6.
17. Webster MA, Hutchinson JN, Rauh MJ, et al. Requirement for both Shc and phosphatidylinositol 3′ kinase signaling pathways in polyomavirus middle T-mediated mammary tumorigenesis. Mol Cell Biol 1998;18:2344–59.
18. Desai KV, Xiao N, Wang W, et al. Initiating oncogenic event determines gene-expression patterns of human breast cancer models. Proc Natl Acad Sci U S A 2002;99:6967–72.
19. Namba R, Maglione JE, Young LJ, et al. Molecular characterization of the transition to malignancy in a genetically engineered mouse-based model of ductal carcinoma *in situ*. Mol Cancer Res 2004;2:453–63.
20. Rosner A, Miyoshi K, Landesman-Bollag E, et al. Pathway pathology: histological differences between ErbB/Ras and Wnt pathway transgenic mammary tumors. Am J Pathol 2002;161:1087–97.
21. Cardiff RD, Anver MR, Gusterson BA, et al. The mammary pathology of genetically engineered mice: the consensus report and recommendations from the Annapolis meeting. Oncogene 2000;19:968–88.
22. Namba R, Young LJ, Maglione JE, et al. Selective estrogen receptor modulators inhibit growth and progression of premalignant lesions in a mouse model of DCIS. Breast Cancer Res 2005;7:R881–9.
23. Jessen KA, Liu SY, Tepper CG, et al. Molecular analysis of metastasis in a polyomavirus middle T mouse model: the role of osteopontin. Breast Cancer Res 2004;6:R157–69.
24. Guy CT, Cardiff RD, Muller WJ. Induction of mammary tumors by expression of polyomavirus middle T oncogene: a transgenic mouse model for metastatic disease. Mol Cell Biol 1992;12:954–61.
25. Rasmussen SB, Young LJT, Smith GH. Preparing mammary gland whole mounts from mice. In: Ip MM, Asch BB, editors. Methods in mammary gland biology and breast cancer research. New York: Kluwer Academic/Plenum Publishers; 2000. p. 67–74.
26. Abbey CK, Borowsky AD, McGoldrick ET, et al. *In vivo* positron-emission tomography imaging of progression and transformation in a mouse model of mammary neoplasia. Proc Natl Acad Sci U S A 2004;101:11438–43.
27. Chatziioannou A, Qi J, Moore A, et al. Comparison of 3-D maximum *a posteriori* and filtered backprojection algorithms for high-resolution animal imaging with microPET. IEEE Trans Med Imaging 2000;19:507–12.
28. Qi J, Leahy RM, Cherry SR, Chatziioannou A, Farquhar TH. High-resolution 3D Bayesian image reconstruction using the microPET small-animal scanner. Phys Med Biol 1998;43:1001–13.
29. Abbey CK, Borowsky AD, McGoldrick ET, et al. PET imaging of development and malignant transformation in a mouse model of mammary intraepithelial neoplasia. Proc SPIE 2005;5746:1–8.
30. Hashemolhosseini S, Nagamine Y, Morley SJ, et al. Rapamycin inhibition of the G_1 to S transition is mediated by effects on cyclin D1 mRNA and protein stability. J Biol Chem 1998;273:14424–9.
31. Guba M, von Breitenbuch P, Steinbauer M, et al. Rapamycin inhibits primary and metastatic tumor growth by antiangiogenesis: involvement of vascular endothelial growth factor. Nat Med 2002;8:128–35.
32. Beuvink I, Boulay A, Fumagalli S, et al. The mTOR inhibitor RAD001 sensitizes tumor cells to DNA-damaged induced apoptosis through inhibition of p21 translation. Cell 2005;120:747–59.
33. Mondesire WH, Jian W, Zhang H, et al. Targeting mammalian target of rapamycin synergistically enhances chemotherapy-induced cytotoxicity in breast cancer cells. Clin Cancer Res 2004;10:7031–42.
34. Zhang PL, Lun M, Siegelmann-Danieli N, Blasick TM, Brown RE. Pamidronate resistance and associated low ras levels in breast cancer cells: a role for combinatorial therapy. Ann Clin Lab Sci 2004;34:263–70.
35. Boulay A, Rudloff J, Ye J, et al. Dual inhibition of mTOR and estrogen receptor signaling *in vitro* induces cell death in models of breast cancer. Clin Cancer Res 2005;11:5319–28.
36. Gera JF, Mellinghoff IK, Shi Y, et al. AKT activity determines sensitivity to mammalian target of rapamycin (mTOR) inhibitors by regulating cyclin D1 and c-myc expression. J Biol Chem 2004;279:2737–46.
37. Peterson RT, Desai BN, Hardwick JS, Schreiber SL. Protein phosphatase 2A interacts with the 70-kDa S6 kinase and is activated by inhibition of FKBP12-rapamycinassociated protein. Proc Natl Acad Sci U S A 1999;96:4438–42.

Clinical Cancer Research

Rapamycin Inhibits Growth of Premalignant and Malignant Mammary Lesions in a Mouse Model of Ductal Carcinoma *In situ*

Ruria Namba, Lawrence J.T. Young, Craig K. Abbey, et al.

Clin Cancer Res 2006;12:2613-2621.